Nuclear pairing: from atomic nuclei to neutron-star crusts

Nicolas Chamel
in collaboration with S. Goriely, J. M. Pearson, A. F. Fantina

Institute of Astronomy and Astrophysics
Université Libre de Bruxelles, Belgium

ESNT - May 29, 2013

Prelude: superfluidity in neutron-star crusts

Describing superfluidity in neutron-star crusts requires a unified understanding of nuclear pairing in both atomic nuclei and nuclear matter.

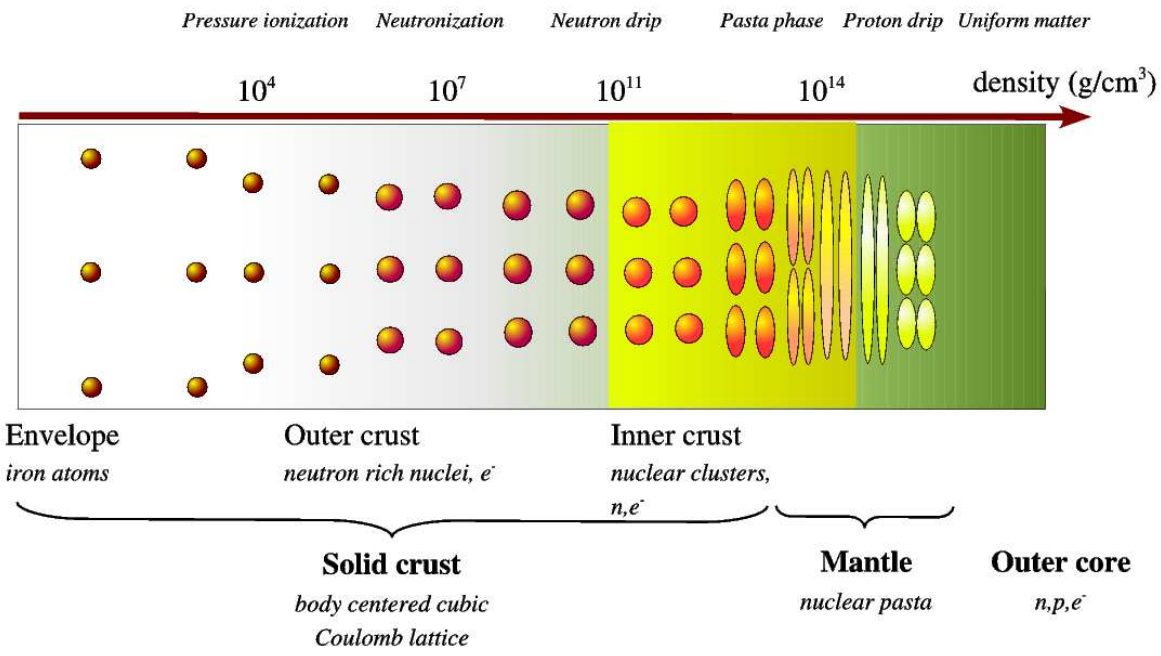

Chamel&Haensel, Living Reviews in Relativity 11 (2008), 10
http://relativity.livingreviews.org/Articles/lrr-2008-10/

Why studying superfluidity in neutron stars?

The interpretation of various observed neutron-star phenomena is affected by superfluidity: pulsar glitches, cooling, pulsar free-precession, quasiperiodic oscillations in soft gamma-ray repeaters, etc.

Page et al., in "Novel Superfluids", Eds. K. H. Bennemann and J. B. Ketterson (2013); arXiv preprint:1302.6626

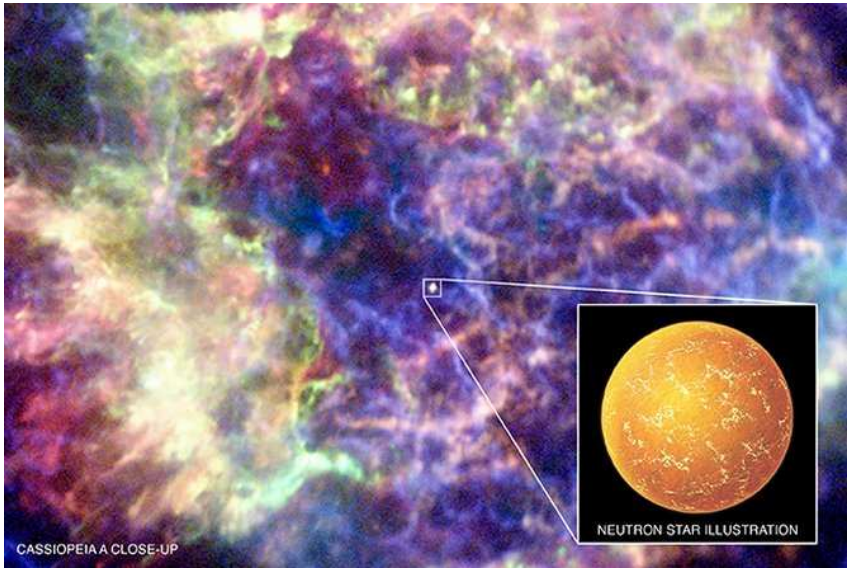

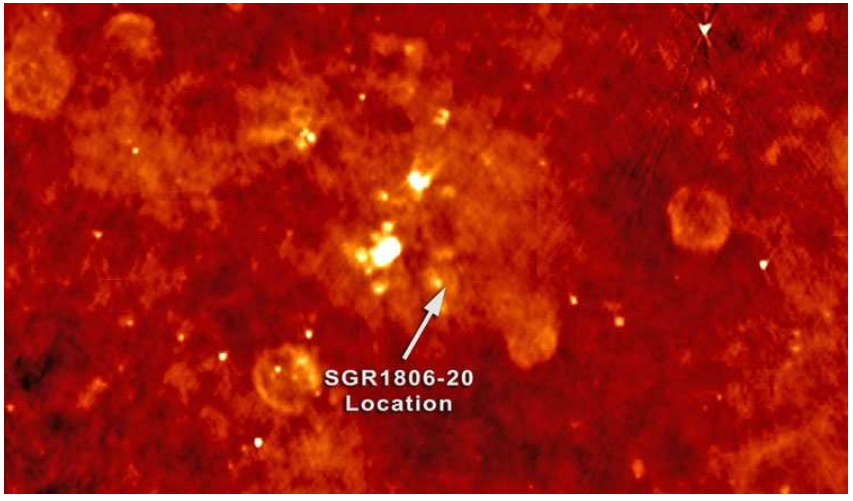

Outline

1. Nuclear energy density functionals for astrophysics
   - fitting protocole of the Brussels-Montreal functionals
   - improved pairing functionals (BSk16-17)
   - (spin-isospin instabilities (BSk18))
   - neutron-matter stiffness (BSk19-21)

2. Applications to neutron-star crusts
   - equilibrium composition
   - superfluidity
   - collective excitations

3. Astrophysical implications
   - nuclear superfluidity and pulsar glitches

Nuclear energy density functionals for astrophysics

Why not using existing Skyrme functionals?

Most of existing Skyrme functionals are not suitable for astrophysics.

- They were adjusted to a few selected nuclei (mostly in the stability valley)
  $\rightarrow$ not suited for investigating stellar nucleosynthesis and the outer crust of neutron stars.
- They were not fitted to the neutron-matter EoS
  $\rightarrow$ not suited for the inner crust of neutron stars.

It is difficult to get physical insight on how to optimize the functional because each one was constructed using a different fitting procedure.

Brussels-Montreal Skyrme functionals (BSk)

Experimental data:

- 2149 atomic masses with $Z, N \geq 8$ from 2003 AME
- compressibility $230 \leq K_v \leq 250$ MeV
- charge radius of ^{208}Pb, $R_c = 5.501 \pm 0.001$ fm
- symmetry energy $J = 30$ MeV

N-body calculations with realistic forces:

- isoscalar effective mass $M_s^*/M = 0.8$
- equation of state of pure neutron matter
- Landau parameters, stability against spurious spin and spin-isospin instabilities
- $^1S_0$ pairing gaps in symmetric and neutron matter

Goriely, Chamel, Pearson, Phys.Rev.C82,035804 (2010).

With these constraints, the functional is well suited for astrophysical applications.

Local pairing energy density functionals

The pairing EDF is very poorly constrained by fitting nuclear masses.

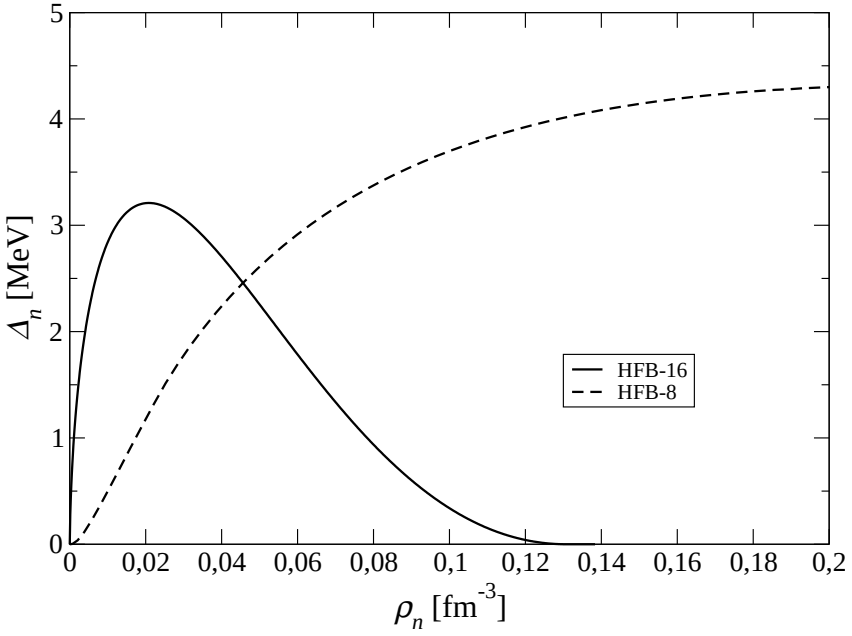

$^1S_0$ pairing gaps in neutron matter for two EDFs, both fitted to nuclear masses: BSk8 (not constrained) and BSk16 (constrained).

Chamel, Goriely, Pearson, Nucl. Phys.A812,72 (2008).

Instead, fit directly the pairing EDF to realistic pairing gaps in infinite nuclear matter.

Empirical pairing energy density functionals

The pairing functional is generally parametrized as

$$\mathcal{E}_{\text{pair}} = \frac{1}{4} \sum_{q=n,p} v^{\pi q}[\rho_n, \rho_p] \tilde{\rho}_q^2$$

$$v^{\pi q}[\rho_n, \rho_p] = V_{\pi q}^{\Lambda} \left(1 - \eta_q \left(\frac{\rho_n + \rho_p}{\rho_0} \right)^{\alpha_q} \right)$$

This functional has to be supplemented with a cutoff prescription.

Drawbacks

- not enough flexibility to fit realistic pairing gaps in infinite nuclear matter and in finite nuclei ($\Rightarrow$ isospin dependence)
- the global fit to nuclear masses would be computationally very expensive

Pairing functionals from nuclear matter calculations

Instead, fit *directly* realistic pairing gaps $\Delta_q(\rho_n, \rho_p)$ in nuclear matter for each densities ρ_n and ρ_p.

Inverting the HFB equations for a *given* pairing gap function Δ_q thus yields

$$v^{\pi q} = -8\pi^2 \left(\frac{\hbar^2}{2M_q^*}\right)^{3/2} \left(\int_0^{\mu_q+\varepsilon_\Lambda} \frac{\sqrt{\varepsilon}\mathrm{d}\varepsilon}{\sqrt{(\varepsilon-\mu_q)^2+\Delta_q(\rho_n,\rho_p)^2}}\right)^{-1}$$

$$\mu_q = \frac{\hbar^2}{2M_q^*}(3\pi^2\rho_q)^{2/3}$$

s.p. energy cutoff ε_Λ above the Fermi level

Chamel, Goriely, Pearson, Nucl. Phys.A812,72 (2008).

Analytical expression of the pairing strength

In the "weak-coupling approximation" $\Delta_q \ll \mu_q$ and $\Delta_q \ll \varepsilon_\Lambda$

$$v^{\pi q} = -\frac{8\pi^2}{\sqrt{\mu_q}} \left(\frac{\hbar^2}{2M_q^*} \right)^{3/2} \left[2 \log \left(\frac{2\mu_q}{\Delta_q} \right) + \Lambda \left(\frac{\varepsilon_\Lambda}{\mu_q} \right) \right]^{-1}$$

$$\Lambda(x) = \log(16x) + 2\sqrt{1+x} - 2 \log \left(1 + \sqrt{1+x} \right) - 4$$

s.p. energy cutoff ε_Λ above the Fermi level

Chamel, Phys. Rev. C 82, 014313 (2010)

- **one-to-one correspondence** between pairing in nuclei and homogeneous nuclear matter
- **no free parameters** apart from the cutoff
- **automatic renormalization** of the pairing strength with ε_Λ

Accuracy of the weak-coupling approximation

This approximation remains very accurate at low densities because the s.p. density of states is not replaced by a constant as usually done.

symmetric nuclear matter

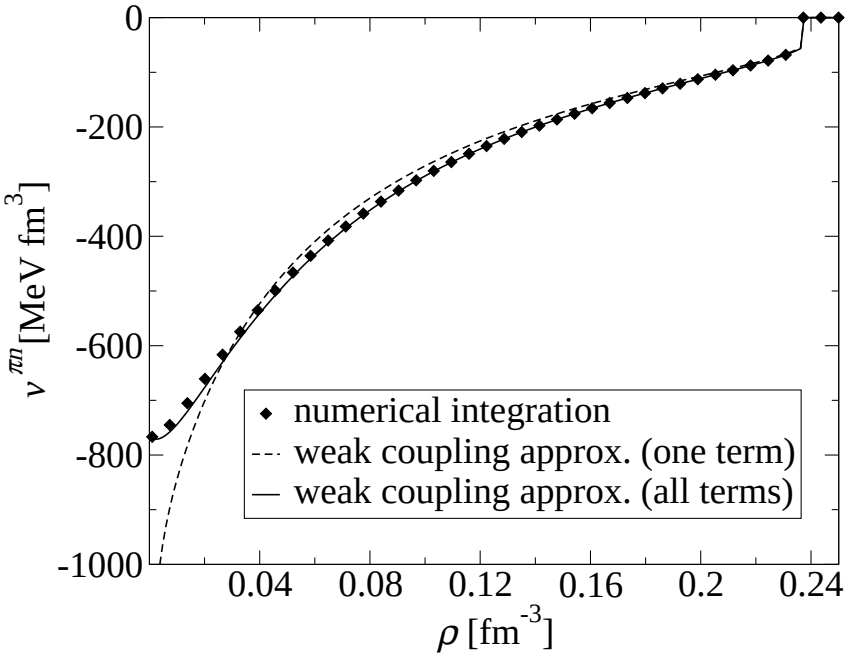

neutron matter

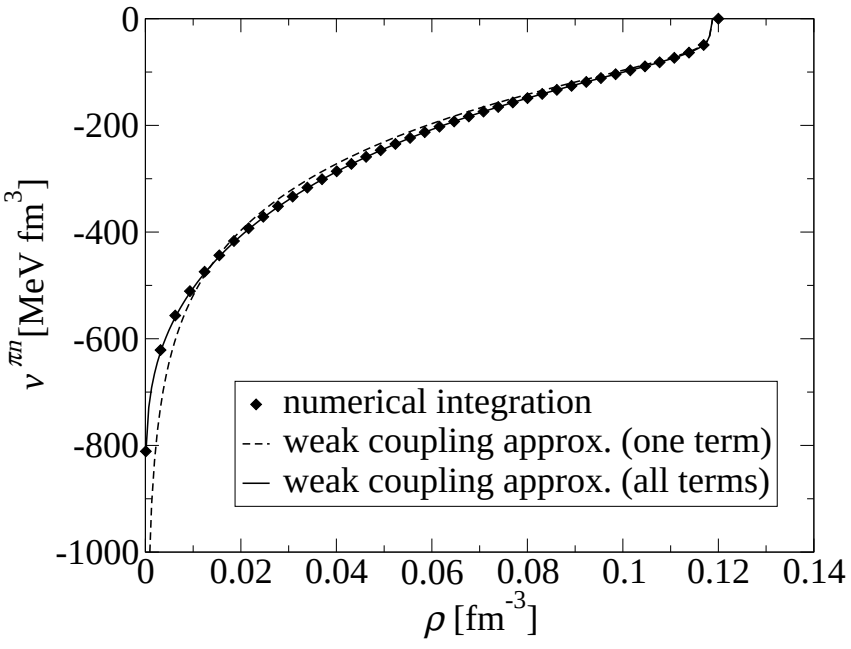

Chamel, Phys. Rev. C 82, 014313 (2010)

Pairing gaps from contact interactions

Conversely, this approximation can be used to obtain the pairing gaps in homogeneous matter from any given contact interaction

$$\Delta = 2\mu \exp\left(\frac{2}{g(\mu)v^{\pi}_{\mathrm{reg}}}\right)$$

μ is the chemical potential, $g(\mu)$ is the density of states and v^{π}_{Λ} is a regularized interaction

$$\frac{1}{v^{\pi}_{\mathrm{reg}}} = \frac{1}{v^{\pi}} + \frac{1}{v^{\pi}_{\Lambda}}$$

$$v^{\pi}_{\Lambda} = \frac{4}{g(\mu)\Lambda(\varepsilon_{\Lambda}/\mu)}$$

Pairing cutoff and experimental phase shifts

In the limit of vanishing density, the pairing strength

$$v^{\pi q}[\rho \to 0] = -\frac{4\pi^2}{\sqrt{\varepsilon_\Lambda}} \left(\frac{\hbar^2}{2M_q} \right)^{3/2}$$

should coincide with the bare force in the $^1S_0$ channel.

A fit to the **experimental $^1S_0$ NN phase shifts** yields $\varepsilon_\Lambda \sim 7 - 8$ MeV.

Esbensen et al., Phys. Rev. C 56, 3054 (1997).

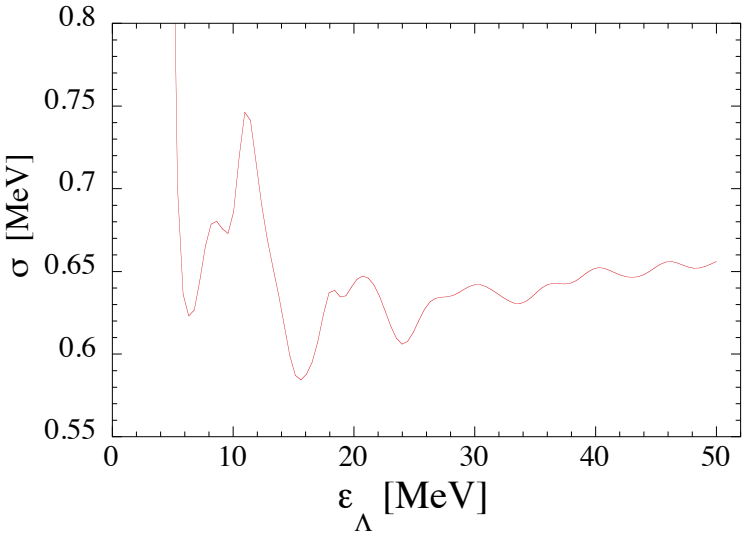

On the other hand, a better mass fit can be obtained with $\varepsilon_\Lambda \sim 16$ MeV

Goriely et al., Nucl.Phys.A773(2006),279.

Chamel et al., arXiv:1204.2076

Other contributions to pairing

In order to take into account

- Coulomb and charge symmetry breaking effects
- polarization effects in odd nuclei (we use the equal filling approximation)
- coupling to surface vibrations

we introduce renormalization factors $f_q^{\pm}$ fitted to nuclear masses

$$v^{\pi n} \longrightarrow f_n^{\pm} v^{\pi n} \ ,$$

$$v^{\pi p} \longrightarrow f_p^{\pm} v^{\pi p} \ .$$

Typically $f_q^{\pm} \simeq 1 - 1.2$ and $f_q^{-} > f_q^{+}$.

HFB-16 and HFB-17 mass models

HFB-16

- $v^{\pi q}[\rho_n, \rho_p] = v^{\pi}[\rho_q]$
- BCS pairing gaps (no medium)
- v^{π} calculated using M_q^*

Chamel, Goriely, Pearson, Nucl. Phys.A812,72 (2008).

HFB-17

- $v^{\pi q}[\rho_n, \rho_p] = v^{\pi q}[\Delta_q(\rho_n, \rho_p)]$
- Brueckner pairing gaps (medium polarization) +interpolation
- v^{π} calculated using M (no self-energy effects on the gap)

Goriely, Chamel, Pearson, PRL102,152503 (2009).

Results of the fit on the 2149 measured masses with $Z, N \geq 8$ from the 2003 Atomic Mass Evaluation:

	HFB-16	HFB-17
σ(2149 M)	**0.632**	**0.581**
$\bar{\epsilon}$(2149 M)	-0.001	-0.019

Neutron-matter equation of state at high densities

We have constructed a family of generalized Skyrme functionals fitted to realistic neutron-matter equations of state with different degrees of stiffness.

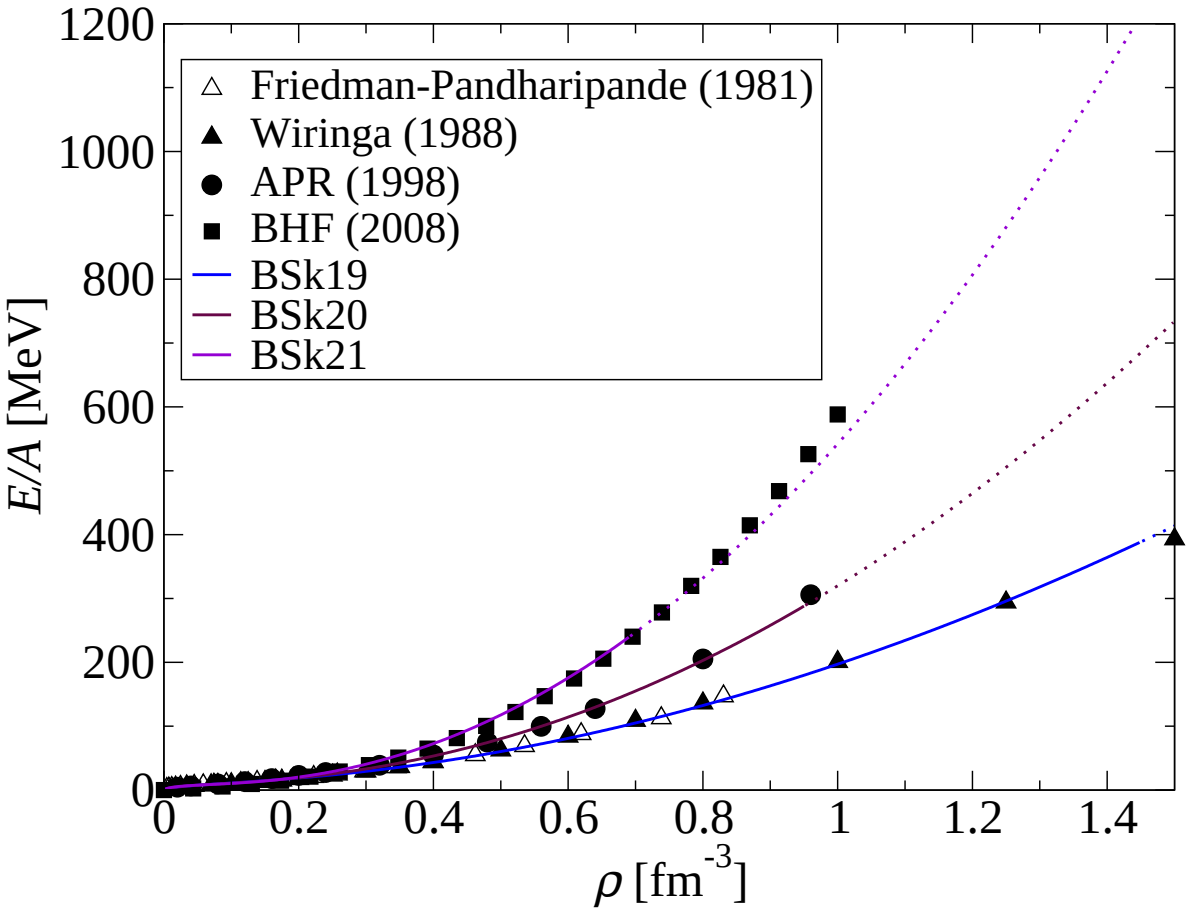

Goriely, Chamel, Pearson, Phys. Rev. C 82, 035804 (2010).

Neutron-matter equation of state at low densities

All three functionals yield similar neutron-matter equations of state at subsaturation densities consistent with microscopic calculations using realistic NN interactions

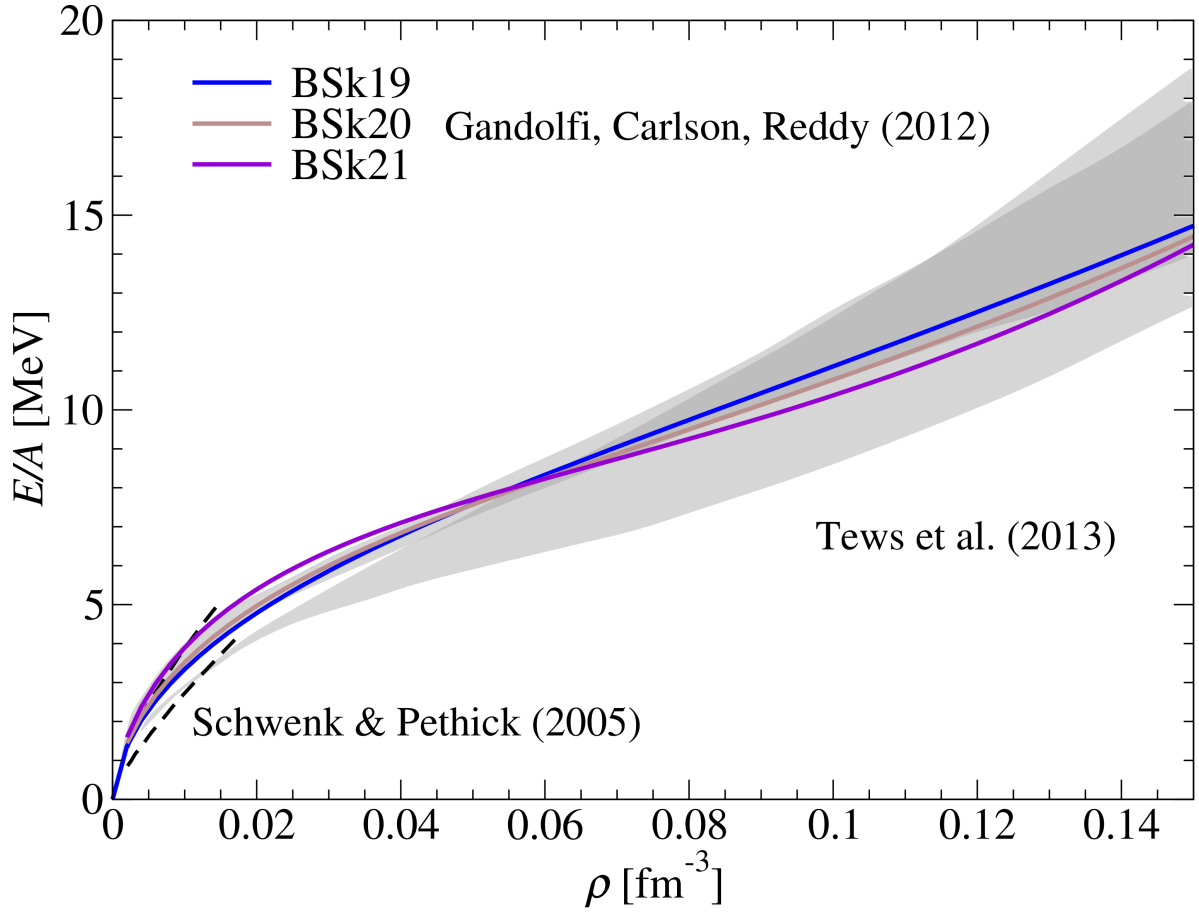

Nuclear-matter equation of state

Our functionals are also in very good agreement with BHF calculations not only in neutron matter but also in symmetric nuclear matter (not fitted).

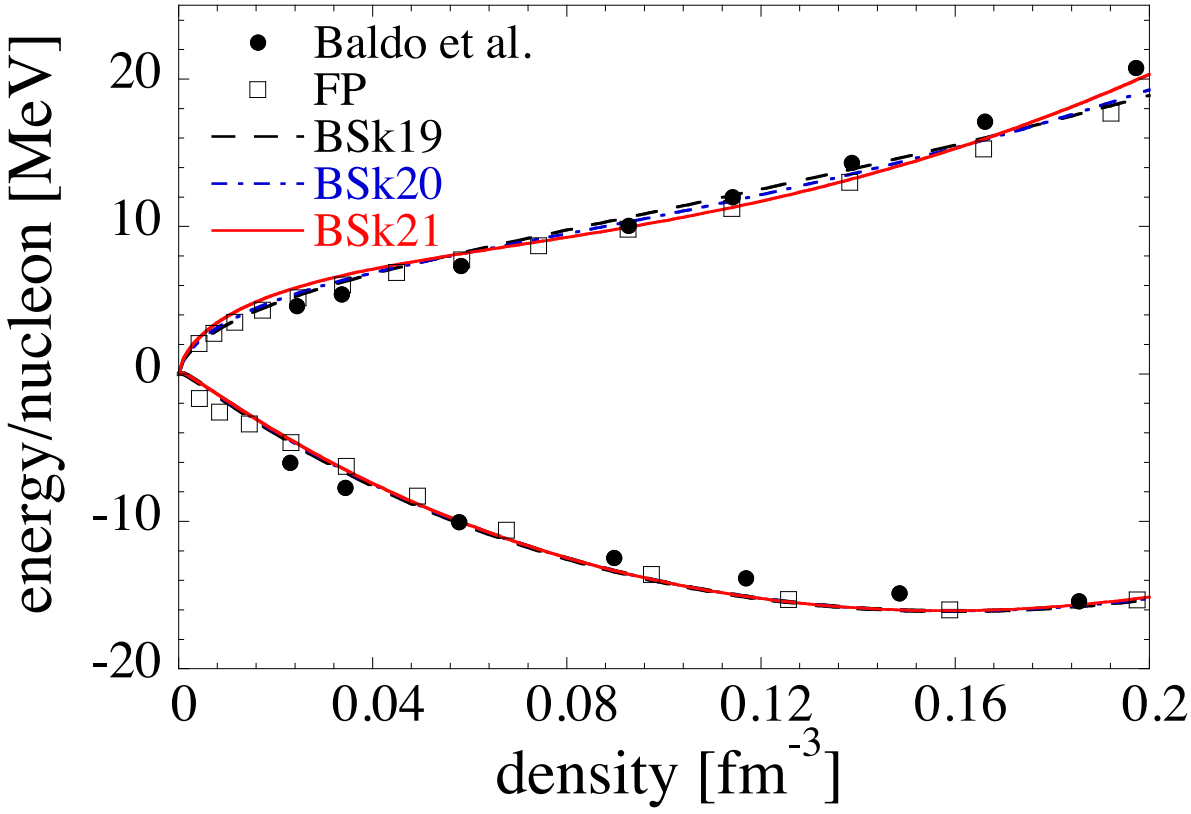

HFB-19,HFB-20 and HFB-21 mass tables

Results of the fit on the 2149 measured masses with $Z, N \geq 8$ from the 2003 Atomic Mass Evaluation
`http://www.astro.ulb.ac.be/bruslib/`

	HFB-19	HFB-20	HFB-21
$\sigma(M)$ [MeV]	0.583	0.583	0.577
$\bar{\epsilon}(M)$ [MeV]	-0.038	0.021	-0.054
$\sigma(M_{nr})$ [MeV]	0.803	0.790	0.762
$\bar{\epsilon}(M_{nr})$ [MeV]	0.243	0.217	-0.086
$\sigma(R_c)$ [fm]	0.0283	0.0274	0.0270
$\bar{\epsilon}(R_c)$ [fm]	-0.0032	0.0009	-0.0014

Goriely, Chamel, Pearson, Phys.Rev.C82,035804(2010).

Comparison with the latest experimental data

Experimental data from the 2011 AME favor HFB-21 (the same trend is observed in the 2012 AME):
`http://www-nds.iaea.org/amdc/`

data set	model	$\bar{\epsilon}(M)$ [MeV]	$\sigma(M)$ [MeV]
2011 AME all (2294)	HFB-21	-0.031	0.574
	HFB-20	-0.010	0.595
	HFB-19	0.051	0.593
2011 AME new (154)	HFB-21	0.185	0.681
	HFB-20	0.375	0.803
	HFB-19	0.310	0.824

HFB-21 is also favored by recent neutron-star mass measurements.

Chamel, Fantina, Pearson, Goriely, Phys.Rev.C84,062802(R)(2011).

Effective masses

Our functionals predict a **qualitatively correct splitting of effective masses** ($M_n^* > M_p^*$ in neutron-rich matter) in agreement with giant resonances and many-body calculations using realistic forces.

$$\frac{M}{M_q^*} = \frac{2\rho_q}{\rho}\frac{M}{M_s^*} + \left(1 - \frac{2\rho_q}{\rho}\right)\frac{M}{M_v^*}$$

	BSk19	BSk20	BSk21	EBHF
M_s^*/M	0.80	0.80	0.80	0.825
M_v^*/M	0.61	0.65	0.71	0.727

BSk21 is also in good **quantitative agreement** with Extended Brueckner Hartree-Fock calculations.

Cao et al.,Phys.Rev.C73,014313(2006).

Applications to neutron star crusts

Description of neutron star crust below neutron drip

Cold catalyzed matter

The interior of a neutron is supposed to be in full thermodynamic equilibrium at zero temperature.

We have determined the equilibrium structure of the outer crust of a neutron star for $\rho \gtrsim 10^4$ g cm^{-3} using the BPS model:

- fully ionized atoms arranged in a bcc lattice
- relativistic electron Fermi gas.

The only microscopic inputs are nuclear masses. We have made use of the experimental data from the 2011 Atomic Mass Evaluation complemented with our HFB mass tables.
Pearson,Goriely,Chamel,Phys.Rev.C83,065810(2011).

Composition of the outer crust of a neutron star

Sequence of equilibrium nuclides with increasing depth:

HFB-19	HFB-20	HFB-21
^{56}Fe	**^{56}Fe**	**^{56}Fe**
^{62}Ni	**^{62}Ni**	**^{62}Ni**
^{64}Ni	**^{64}Ni**	**^{64}Ni**
^{66}Ni	**^{66}Ni**	**^{66}Ni**
^{86}Kr	**^{86}Kr**	**^{86}Kr**
^{84}Se	**^{84}Se**	**^{84}Se**
^{82}Ge	**^{82}Ge**	**^{82}Ge**
^{80}Zn	**^{80}Zn**	**^{80}Zn**
^{82}Zn	^{82}Zn	-
-	-	^{79}Cu
	^{78}Ni	^{78}Ni
^{80}Ni	^{80}Ni	^{80}Ni
^{126}Ru	^{126}Ru	-
^{124}Mo	^{124}Mo	^{124}Mo
-	^{122}Mo	-
^{122}Zr	^{122}Zr	^{122}Zr
^{124}Zr	^{124}Zr	-
-	-	^{121}Y
^{120}Sr	^{120}Sr	^{120}Sr
^{122}Sr	^{122}Sr	^{122}Sr
^{124}Sr	^{124}Sr	^{124}Sr
^{126}Sr	^{126}Sr	-

- **The first 8 nuclides are determined by experimental masses.**
- **Predominance of $N \sim 50$ and ~ 82 nuclei.**

Deeper (below $\sim$ 200 m for a $1.4M_{\odot}$ neutron star with a 10 km radius) the composition is more model-dependent. Measurements of neutron-rich nuclei are crucially needed.
Pearson,Goriely,Chamel,Phys.Rev.C83,065810.
Wolf et al.,PRL110,041101.

Description of neutron star crust beyond neutron drip

We have determined the equilibrium structure of the inner crust of a neutron star for $\rho \gtrsim 4 \times 10^{11}$g cm^{-3} using the Extended Thomas-Fermi+Strutinsky Integral method (ETFSI):

- spherical neutron-proton clusters coexisting with a neutron liquid (Wigner-Seitz approximation used to compute the Coulomb energy)
- relativistic electron Fermi gas.

Pearson,Chamel,Goriely,Ducoin,Phys.Rev.C85,065803(2012).

Advantages of ETFSI method

- very fast approximation to the full Hartree-Fock method
- avoids the difficulties related to boundary conditions but include proton shell effects (neutron shell effects are much smaller and are therefore omitted)
  Chamel et al.,Phys.Rev.C75(2007),055806.

Structure of the inner crust of a neutron star (I) nucleon distributions

With increasing density, the clusters keep essentially the same size but become more and more dilute:

Crust-core transition properties

	$\bar{n}_{cc}$ (fm^{-3})	P_{cc} (MeV fm^{-3})
BSk19	0.0885	0.428
BSk20	0.0854	0.365
BSk21	0.0809	0.268
SLy4	0.0798	0.361

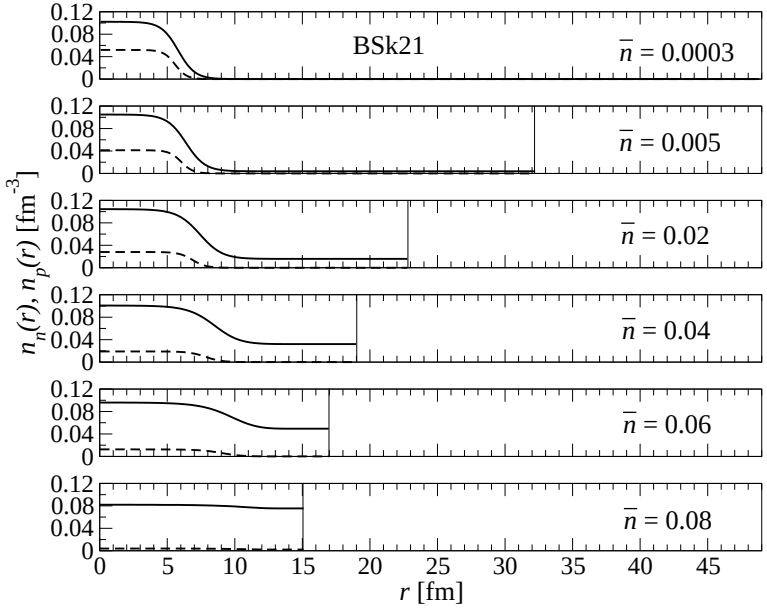

The crust-core transition is very smooth: the crust dissolves continuously into a uniform mixture of nucleons and electrons.

Structure of the inner crust of a neutron star (II) composition

ETFSI calculations for two different functionals

with BSk14

$\bar{n}$ (fm^{-3})	Z	A
0.0003	50	200
0.001	50	460
0.005	50	1140
0.01	40	1215
0.02	40	1485
0.03	40	1590
0.04	40	1610
0.05	20	800
0.06	20	780

with BSk17

$\bar{n}$ (fm^{-3})	Z	A
0.0003	50	190
0.001	50	432
0.005	50	1022
0.01	50	1314
0.02	40	1258
0.03	40	1334
0.04	40	1354
0.05	40	1344
0.06	40	1308

With BSk19, BSk20 and BSk21, only $Z = 40$ is found.

Structure of the inner crust of a neutron star (II) composition

- The ordinary nuclear shell structure seems to be preserved apart from $Z = 40$ (quenched spin-orbit?).
- The energy differences between different configurations become very small as the density increases:

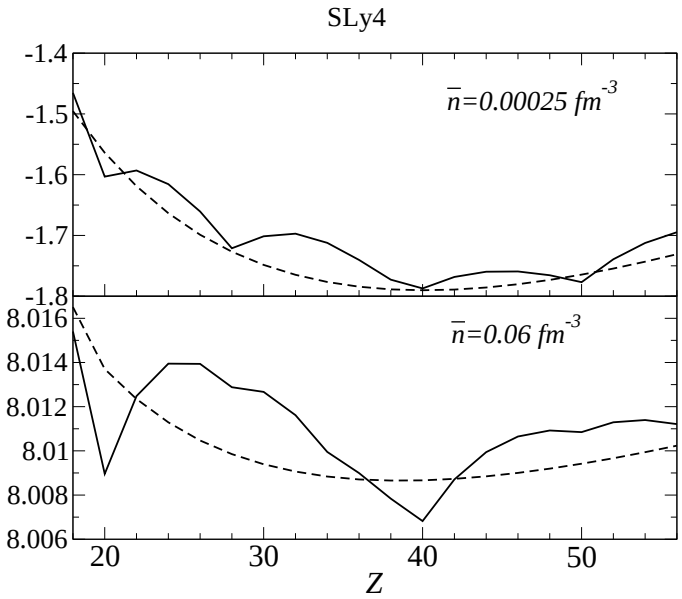

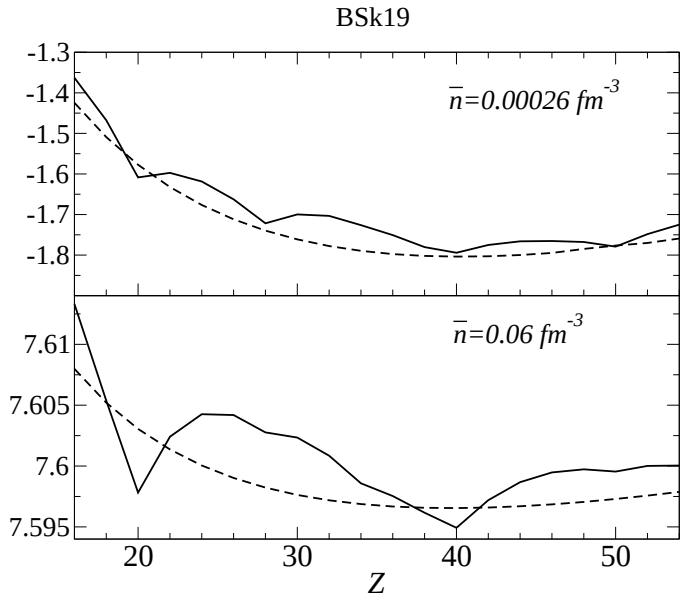

In a real neutron star, a large range of values of Z can be expected due to thermal effects.

Structure of the inner crust of a neutron star (III) composition

Impact of proton pairing (BCS approximation) - preliminary results with BSk21

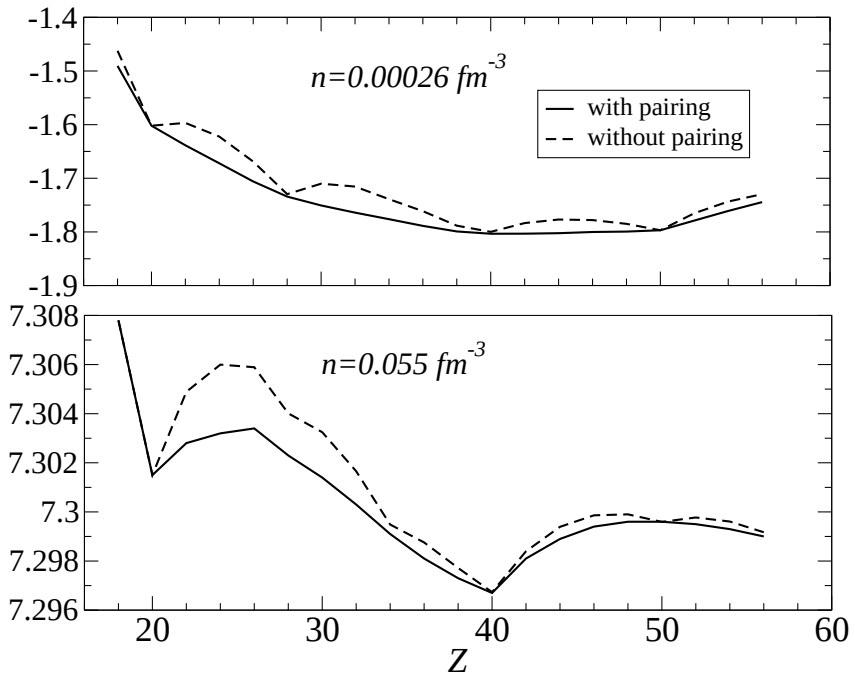

Even though pairing smoothes out shell effects, it does not change appreciably the composition.

Superfluidity in neutron-star crusts with the Wigner-Seitz approximation

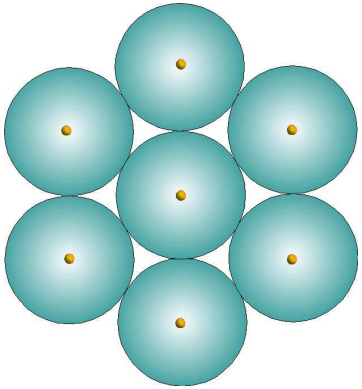

Pairing properties have been already studied using the HFB method and the Wigner-Seitz approximation.

However, this approach is not well suited for treating the deep region of the crust

Chamel et al., Phys.Rev.C75(2007)055806.

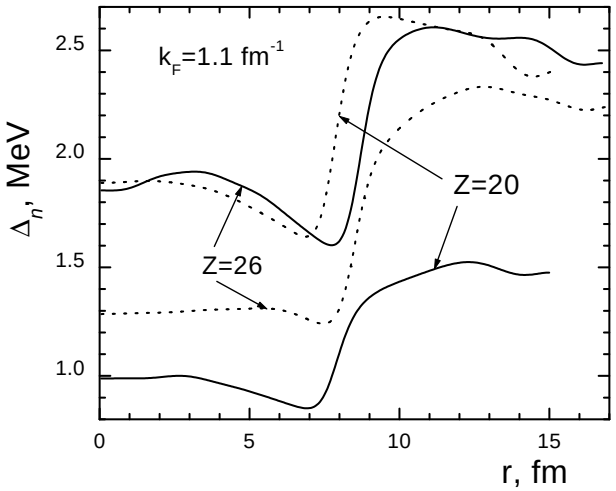

Spurious shell effects $\propto 1/R^2$ can be very large at the crust bottom and are enhanced by the self-consistency.

Baldo et al., Eur.Phys.J. A 32, 97(2007).

Nuclear band theory

Long-range correlations can be taken into account using the band theory of solids

Chamel et al., Phys.Rev.C75(2007)055806.

Band theory of solids in a nut shell:

$$\varphi_{\alpha \boldsymbol{k}}(\boldsymbol{r}) = e^{\mathrm{i}\boldsymbol{k}\cdot\boldsymbol{r}} u_{\alpha \boldsymbol{k}}(\boldsymbol{r})$$

$$u_{\alpha \boldsymbol{k}}(\boldsymbol{r} + \boldsymbol{T}) = u_{\alpha \boldsymbol{k}}(\boldsymbol{r})$$

- $\alpha \rightarrow$ rotational symmetry around lattice sites (clusters)
- $\boldsymbol{k} \rightarrow$ translational symmetry (unbound neutrons)

Example of neutron band structure

Body-centered cubic crystal of zirconium like clusters with $N = 160$ (70 unbound) and $\bar{\rho} = 7 \times 10^{11}$ g.cm^{-3}

W-S approximation

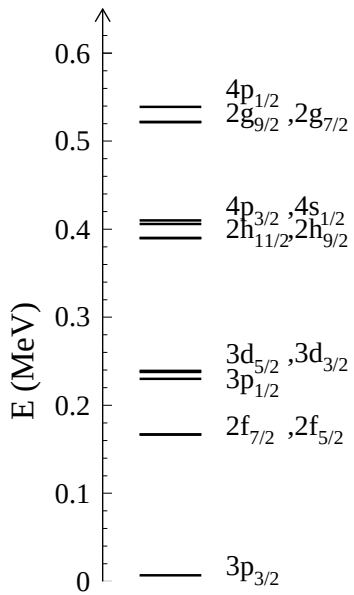

band theory

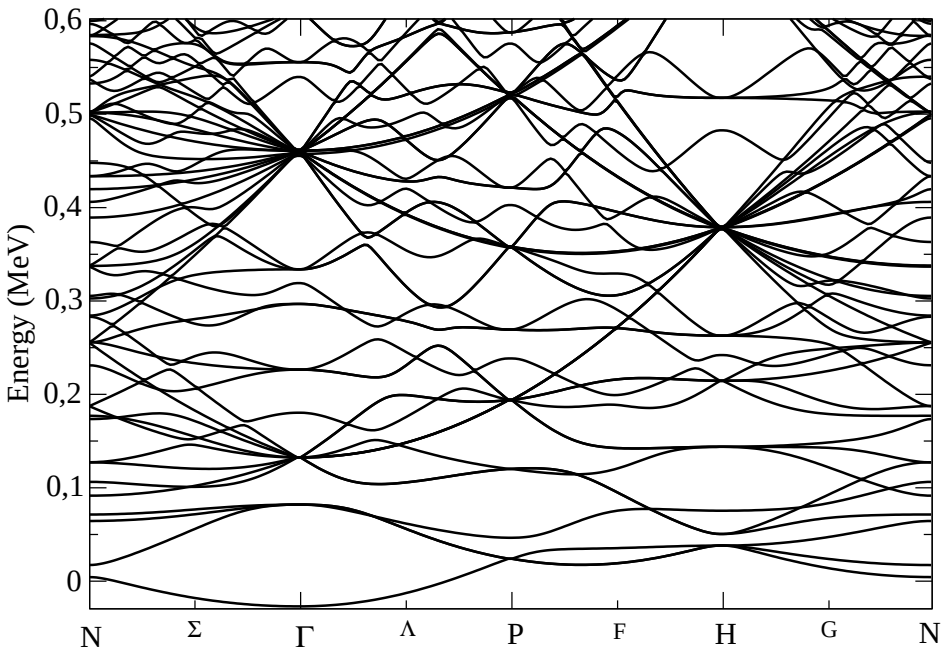

Chamel et al, Phys.Rev.C75 (2007), 055806

Anisotropic multi-band neutron superfluidity

In the decoupling approximation, the Hartree-Fock-Bogoliubov equations reduce to the BCS equations

$$\Delta_{\alpha\boldsymbol{k}} = -\frac{1}{2}\sum_{\beta}\sum_{\boldsymbol{k}'} \bar{v}^{\mathrm{pair}}_{\alpha\boldsymbol{k}\alpha-\boldsymbol{k}\beta\boldsymbol{k}'\beta-\boldsymbol{k}'} \frac{\Delta_{\beta\boldsymbol{k}'}}{E_{\beta\boldsymbol{k}'}} \tanh\frac{E_{\beta\boldsymbol{k}'}}{2T}$$

$$\bar{v}^{\mathrm{pair}}_{\alpha\boldsymbol{k}\alpha-\boldsymbol{k}\beta\boldsymbol{k}'\beta-\boldsymbol{k}'} = \int \mathrm{d}^3r\, v^{\pi}[\rho_n(\boldsymbol{r}),\rho_p(\boldsymbol{r})]\,|\varphi_{\alpha\boldsymbol{k}}(\boldsymbol{r})|^2|\varphi_{\beta\boldsymbol{k}'}(\boldsymbol{r})|^2$$

$$E_{\alpha\boldsymbol{k}} = \sqrt{(\varepsilon_{\alpha\boldsymbol{k}}-\mu)^2+\Delta^2_{\alpha\boldsymbol{k}}}$$

$\varepsilon_{\alpha\boldsymbol{k}}$, μ and $\varphi_{\alpha\boldsymbol{k}}(\boldsymbol{r})$ are obtained from band structure calculations

Chamel et al., Phys.Rev.C81,045804 (2010).

Analogy with terrestrial multi-band superconductors

Multi-band superconductors were first studied by Suhl et al. in 1959 but clear evidence were found only in 2001 with the discovery of MgB_2 (two-band superconductor)

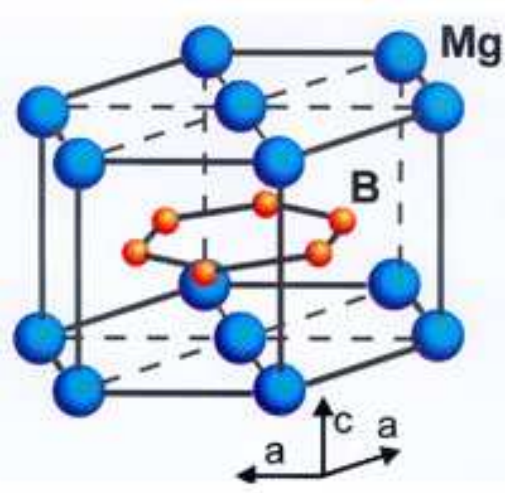

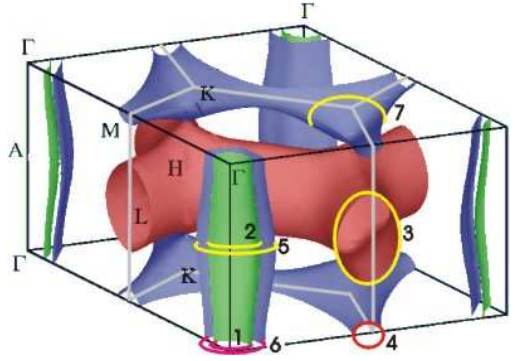

In neutron-star crusts,

- the number of bands can be huge $\sim$ up to a thousand!
- both intra- and inter-band couplings must be taken into account

Neutron pairing gaps

Example at $\bar{n} = 0.06$ fm^{-3} with BSk16

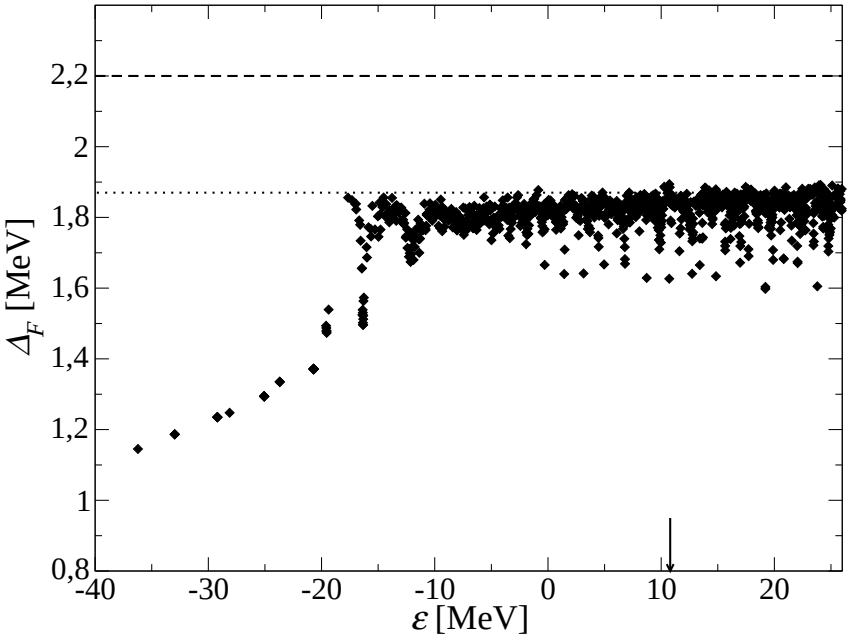

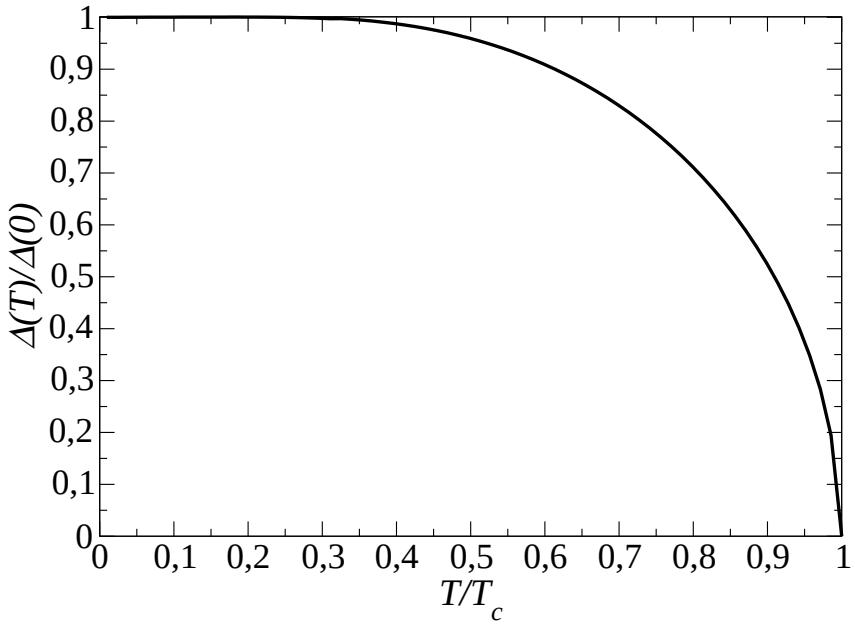

- $\Delta_{\alpha \boldsymbol{k}}(T)/\Delta_{\alpha \boldsymbol{k}}(0)$ is a universal function of T
- The critical temperature is approximately given by the usual BCS relation $T_c \simeq 0.567\Delta_F$

Neutron pairing gaps vs density

n_n^f is the density of unbound neutrons
$\Delta_{\rm u}$ is the gap in neutron matter at density n_n^f
$\bar{\Delta}_{\rm u}$ is the gap in neutron matter at density n_n

$\bar{n}$ [fm^{-3}]	Z	A	n_n^f [fm^{-3}]	$\Delta_{\rm F}$ [MeV]	$\Delta_{\rm u}$ [MeV]	$\bar{\Delta}_{\rm u}$ [MeV]
0.07	40	1218	0.060	1.44	1.79	1.43
0.065	40	1264	0.056	1.65	1.99	1.65
0.06	40	1260	0.051	1.86	2.20	1.87
0.055	40	1254	0.047	2.08	2.40	2.10
0.05	40	1264	0.043	2.29	2.59	2.33

- the nuclear clusters lower the gap by 10 – 20%
- both bound and unbound neutrons contribute to the gap

Pairing field and local density approximation

The effects of inhomogeneities on neutron superfluidity can be directly seen in the pairing field

$$\Delta_n(\boldsymbol{r}) = -\frac{1}{2} v^{\pi n}[\rho_n(\boldsymbol{r}), \rho_p(\boldsymbol{r})]\tilde{\rho}_n(\boldsymbol{r}), \;\; \tilde{\rho}_n(\boldsymbol{r}) = \sum_{\alpha,\boldsymbol{k}}^{\Lambda} |\varphi_{\alpha\boldsymbol{k}}(\boldsymbol{r})|^2 \frac{\Delta_{\alpha\boldsymbol{k}}}{E_{\alpha\boldsymbol{k}}}$$

Neutron pairing field for $\bar{n} = 0.06$ fm^{-3} at $T = 0$

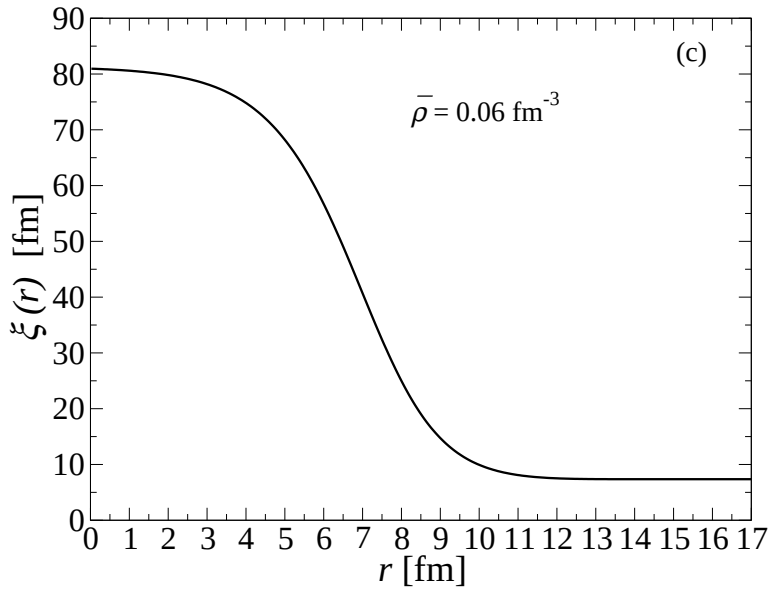

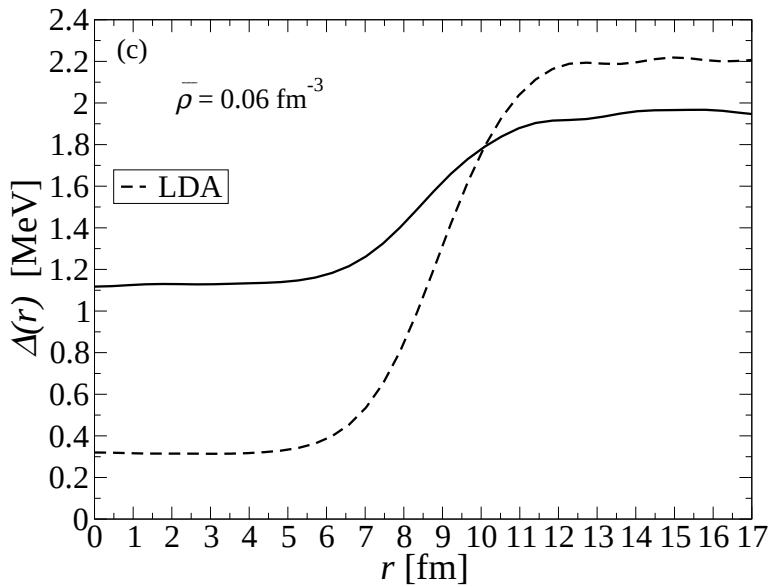

Chamel et al., Phys.Rev.C81(2010)045804.

Impact of the pairing cutoff

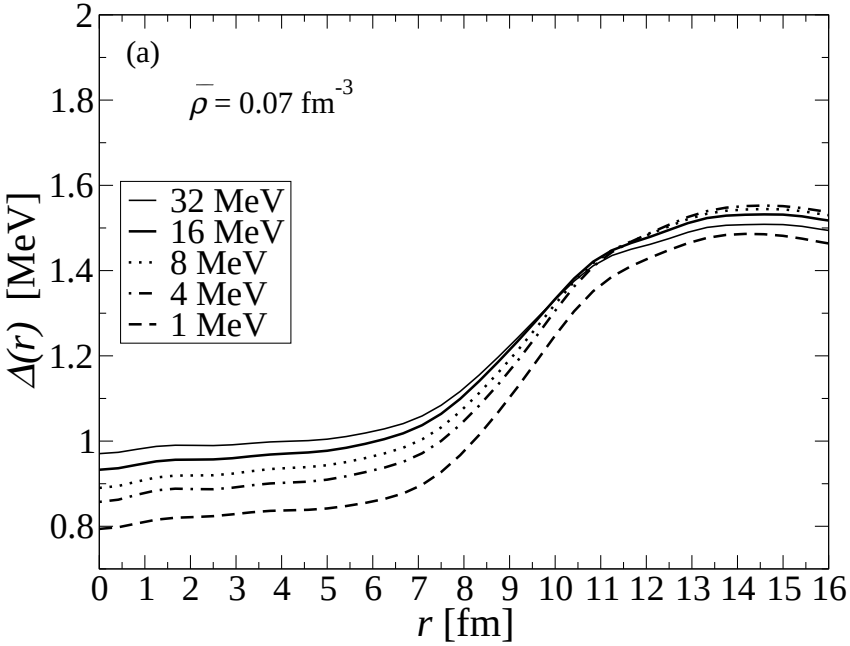

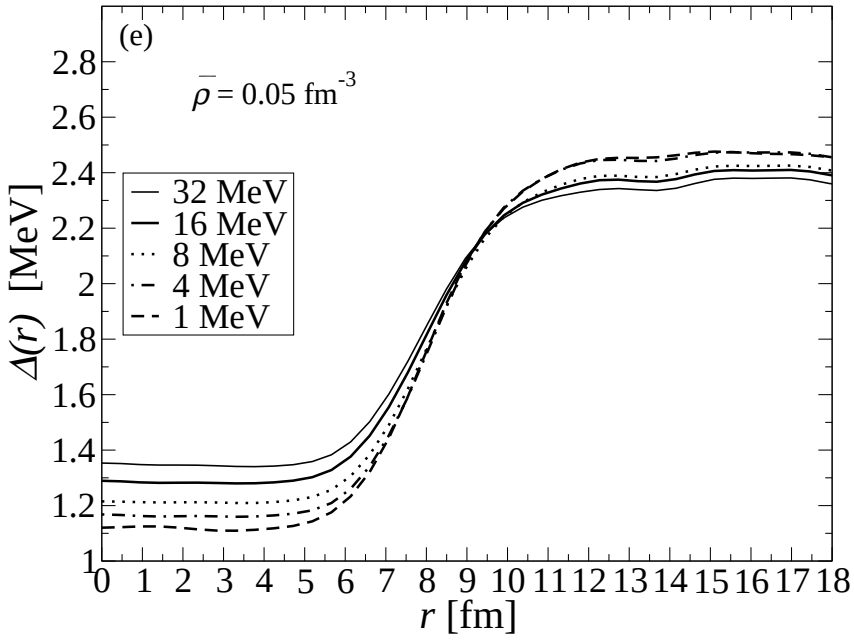

$\bar{n}$ [fm^{-3}]	$\Delta_{F0}(16)$ [MeV]	$\Delta_{F0}(8)$	$\Delta_{F0}(4)$	$\Delta_{F0}(2)$	$\Delta_{F0}(1)$
0.070	1.39	1.38	1.37	1.36	1.29
0.050	2.27	2.25	2.27	2.26	2.24

Pairing gaps (hence also critical temperatures) are very weakly dependent on the pairing cutoff.

Pairing in the shallow region of the inner crust

3D HFB calculations using the *fixed* (ETFSI) mean field with Bloch boundary conditions. Preliminary results.

Example for ^{185}Sn at $\bar{n} = 0.0003$ fm^{-3} with BSk16

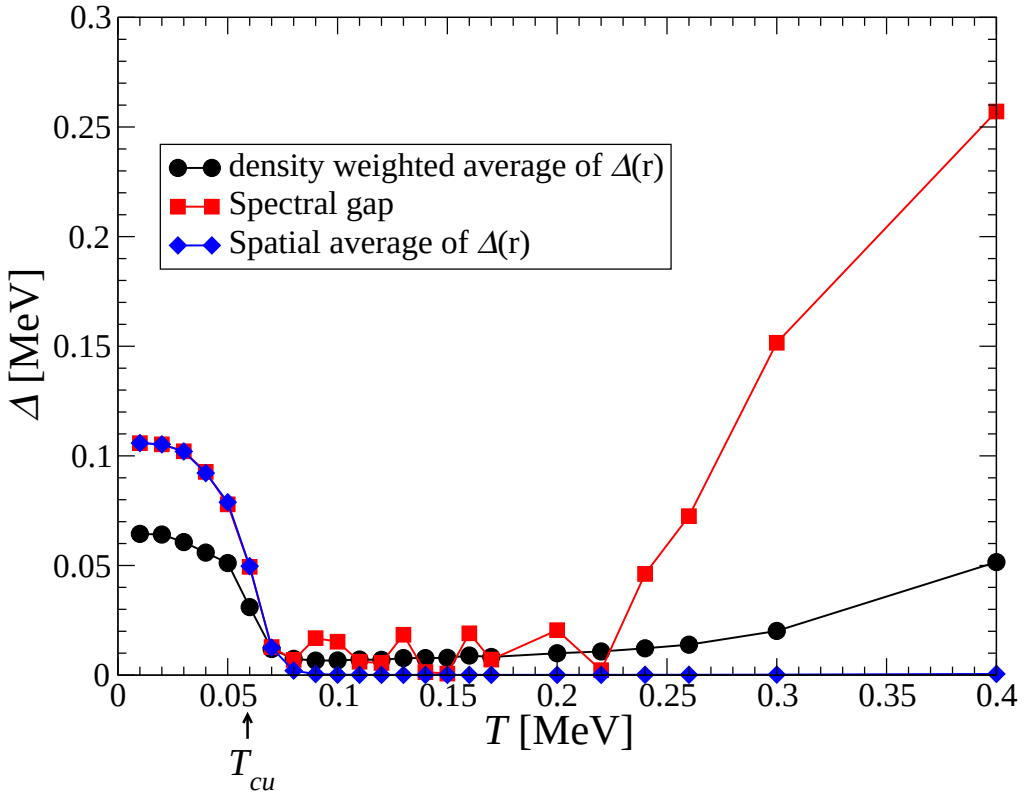

Pairing is enhanced for $T > T_c$! This agrees with recent calculations from *Margueron& Khan, Phys.Rev.C86,065801(2012).*

Entrainment

Despite the absence of viscous drag, the crust can still resist the flow of the neutron superfluid due to non-local and non-dissipative entrainment effects.

Carter, Chamel and Haensel, Nucl.Phys.A748,675(2005).

Neutrons with specific wavevectors $\boldsymbol{k}$ can be elastically scattered by the lattice: this is Bragg diffraction. This occurs if

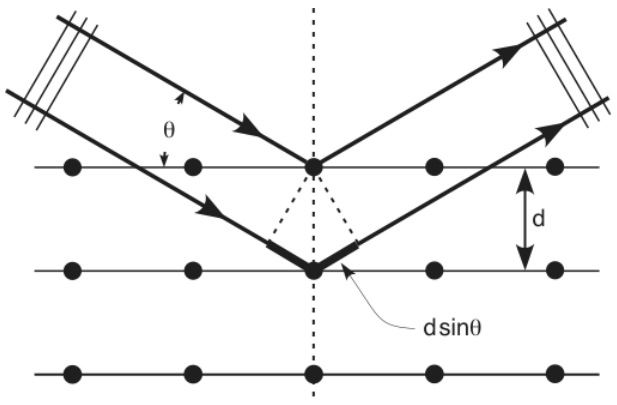

$$2d \sin\theta = N\lambda$$

- Neutrons that are reflected do not propagate: $\boldsymbol{v} = 0$
- Others do propagate but with $\boldsymbol{v} = \hbar\boldsymbol{k}/m_n^\star$

How “free” are neutrons in neutron-star crusts?

On average $m_n^\star \gg 1$ so that most neutrons are actually entrained by the crust

Chamel,Phys.Rev.C85,035801(2012).

n_b (fm^{-3})	n_n^f/n_n (%)	n_n^c/n_n^f (%)
0.0003	20.0	82.6
0.001	68.6	27.3
0.005	86.4	17.5
0.01	88.9	15.5
0.02	90.3	7.37
0.03	91.4	7.33
0.04	88.8	10.6
0.05	91.4	30.0
0.06	91.5	45.9
0.08	104	64.8

The density $n_n^c = n_n^f/m_n^\star$ of “conduction” neutrons (i.e. superfluid neutron density) can be much smaller than the density n_n^f of free neutrons!

Low-energy collective excitations

Due to entrainment, the Bogoliubov-Anderson bosons are strongly mixed with lattice phonons.

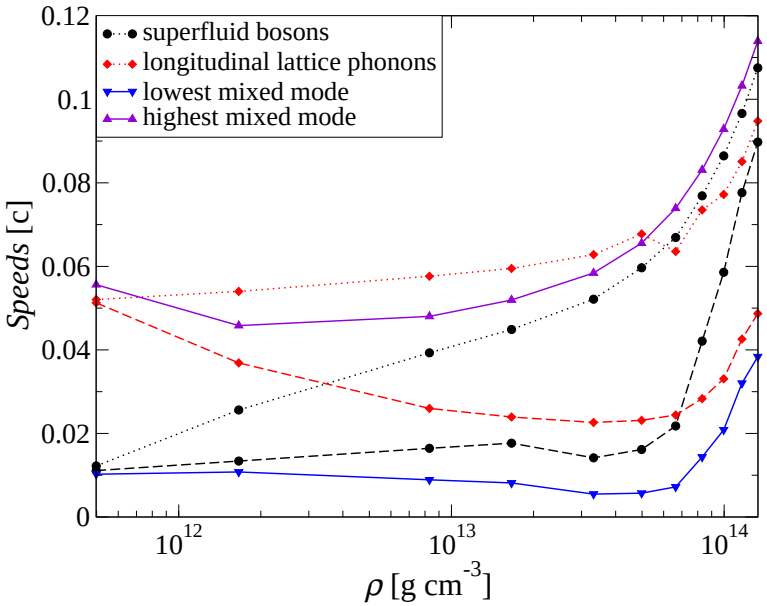

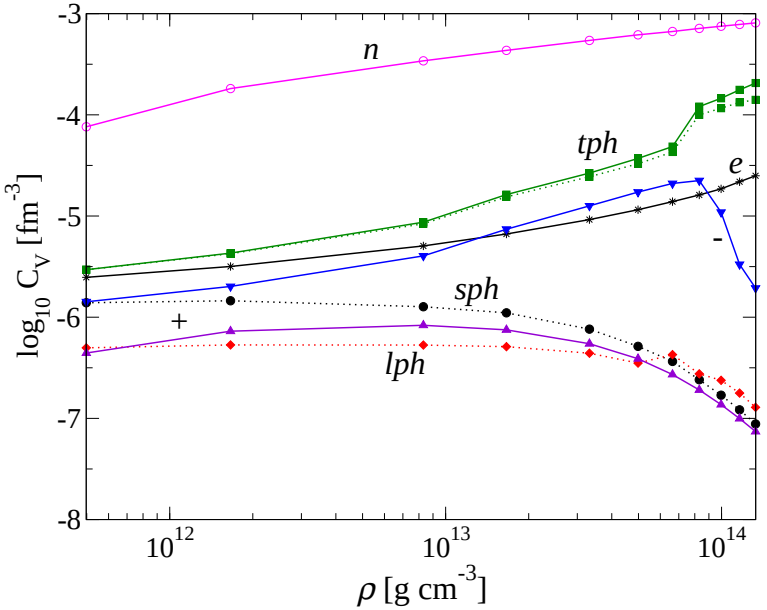

The contribution of superfluid neutrons to the crustal specific heat is neglibly small. But with entrainment, the contribution of longitudinal modes can be nonnegligible.

Chamel,Page,Reddy,Phys.Rev.C87,035803(2013).

Astrophysical implications

Pulsar glitches and superfluidity

Sometimes pulsars may suddenly spin up. These glitches are followed by a relaxation over days to years thus hinting at the superfluidity in neutron stars.

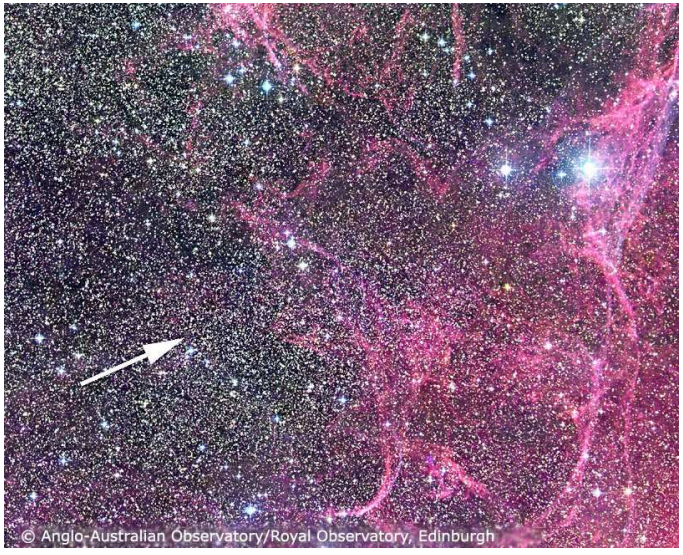

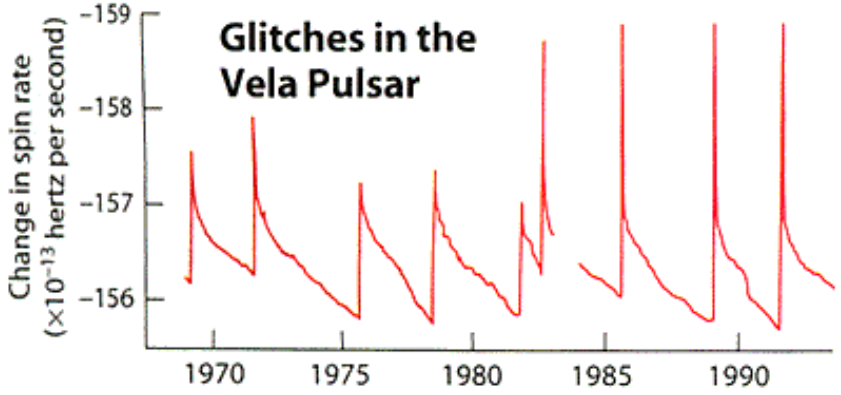

Superfluidity is also expected to play a key role in the mechanism of large glitches (e.g. catastrophic unpinning of superfluid vortices).

Anderson and Itoh, Nature 256, 25 (1975)

Pulsar glitches and entrainment

Glitches are usually interpreted as **sudden tranfers of angular momentum between the superfluid in the crust and the rest of star**. However this superfluid is also entrained !

$$\begin{aligned} J_s &= I_{ss}\Omega_f + I_{sc}\Omega_c \\ J_c &= I_{cc}\Omega_c + I_{sc}\Omega_f \end{aligned} \Rightarrow \frac{(I_s)^2}{I_{ss}I} \geq A_g \frac{\Omega}{|\dot{\Omega}|}, \qquad A_g = \frac{1}{t}\sum_i \frac{\Delta\Omega_i}{\Omega}$$

Chamel&Carter,MNRAS368,796(2006)

Application to the Vela pulsar:

$$A_g \simeq 2.25 \times 10^{-14}\ \mathrm{s}^{-1}$$

$$\frac{(I_s)^2}{I_{ss}I} \geq 1.6\%$$

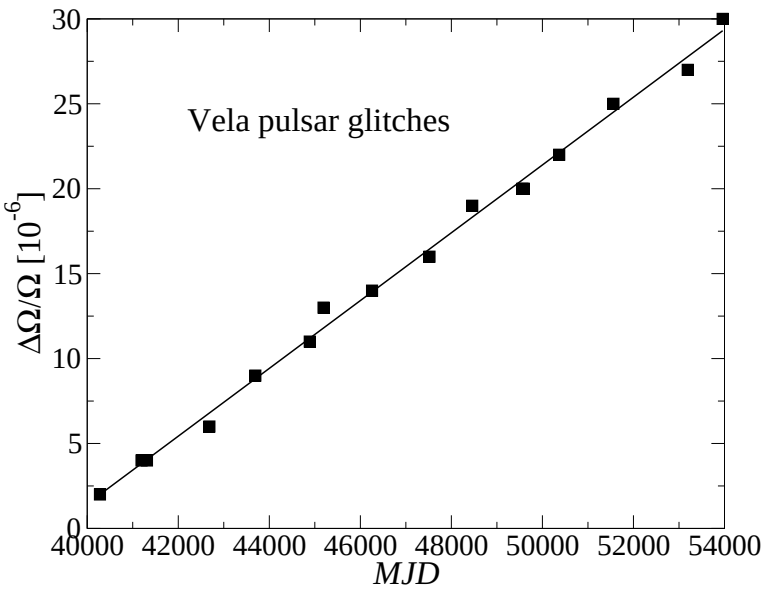

Pulsar glitch constraint

Shaded areas are excluded if Vela pulsar glitches originate in the crust.

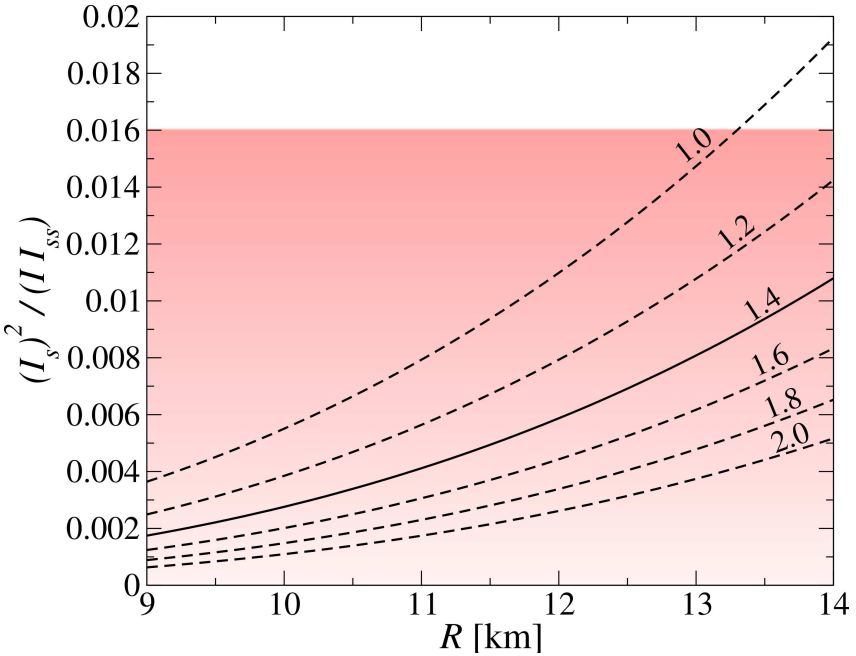

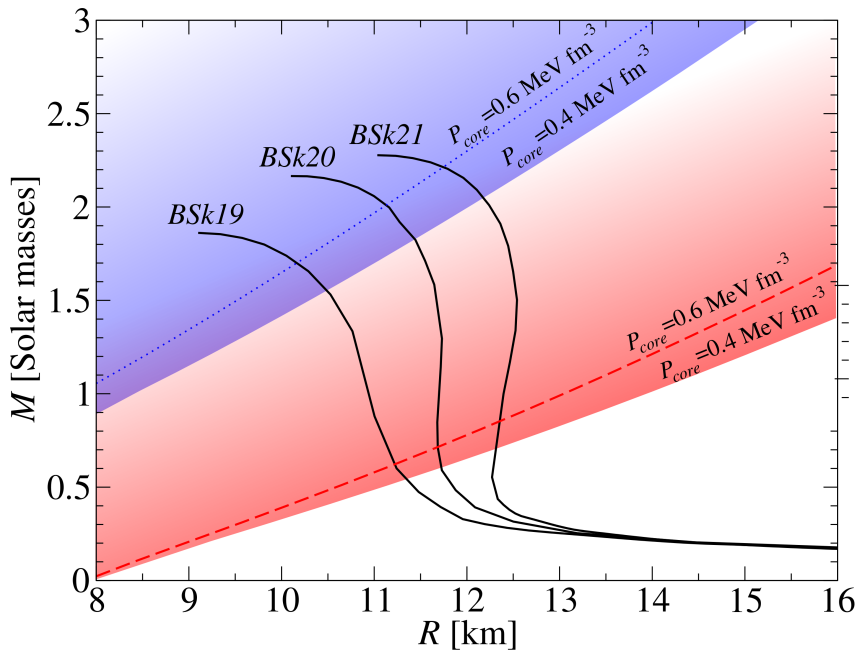

The inferred mass of Vela is unrealistically low $M < M_{\odot}$.

Due to entrainment, the superfluid in the crust does not carry enough angular momentum to explain large glitches.

Chamel, PRL 110, 011101(2013).

Summary

In order to study pairing in neutron-star crusts,

1. we have developed generalized Skyrme EDF constrained by experiments and N-body calculations:
   - they give an excellent fit to essentially all mass data ($\sigma \lesssim 0.6$ MeV)
   - they reproduce various properties of homogeneous nuclear matter (EoS, $^1S_0$ pairing gaps, effective masses *etc*)
2. we have implemented the band theory of solids (long-range correlations).

We find that the neutron superfluid and the crust are strongly coupled, and this has astrophysical implications.

Open issues: contribution of collective excitations to pairing, impact of quantum and thermal fluctuations, impurities, lattice defects etc.